J Appl Electrochem (2009) 39:1217–1227
DOI 10.1007/s10800-009-9777-6

ORIGINAL PAPER

Silver–copper electrodeposition from ammonium hydroxide solution: influence of EDTA and HEDTA

G. M. de Oliveira · I. A. Carlos

Received: 2 April 2008 / Accepted: 5 January 2009 / Published online: 23 January 2009

Abstract The influence of EDTA (ethylenediaminetetraacetic acid, disodium salt) or HEDTA (N-(2-hydroxyethyl) ethylenediaminetriacetic acid, trisodium salt) on silver–copper electrodeposition from ammonium hydroxide solution was investigated. Voltammetric studies showed that silver was deposited at potentials more negative than +0.100 V, while the copper(II) ion was reduced to copper(I) ion and metallic copper at potentials more negative than +0.100 and −0.375 V, respectively. Chronoamperometry, scanning electron microscopy and energy-dispersive X-ray spectroscopy (EDS) indicated that, for deposits obtained at −0.450 V, increasing either the silver content in the silver–copper deposit or the charge density of deposition led to dendritic growth. Moreover, dendritic growth decreased when either the EDTA or HEDTA concentration increased. EDS analysis of the deposits obtained at −0.200 V showed codeposition of copper with silver, which was attributed to Cu(I) ion disproportionation to Cu(0) and Cu(II). Moreover, the silver–copper deposits obtained at −0.200 V, from a solution containing EDTA or HEDTA, were non-dendritic in spite of the high silver content. The presence of EDTA and HEDTA improved the silver–copper morphology. X-ray diffraction analysis indicated that the silver–copper electrodeposit was a supersaturated solid solution.

Keywords Silver–copper · Additive · Alloy · Electrodeposition · Supersaturated solid solution

G. M. de Oliveira · I. A. Carlos (✉)
Chemistry Department, Federal University of São Carlos, CP 676, 13565-905 São Carlos, SP, Brazil
e-mail: diac@ufscar.br

1 Introduction

Silver–copper alloy is an interesting material since it exhibits excellent electrical and thermal conductivity, good corrosion resistance, malleability and ductility. These features allow application of silver–copper alloys in a wide range of industrial situations, for example, on electrical circuit boards, capacitor components, thin-film coatings for optically and thermally efficient glasses, telephone relay contacts, electromagnetic launcher conductor materials and nanoparticles for lead-free interconnect solders, etc. [1–3].

Copper and silver are normally immiscible metals, producing a eutectic solution at 28.1 wt% copper [4]. However, by quenching methods, it is possible to obtain a supersaturated solid solution of silver–copper with various silver/copper ratios [5], in the form of a disordered fcc alloy (γ phase) or an amorphous alloy [6]. Electrodeposition can also lead to supersaturated alloys.

Silver–copper electrodeposition is a poorly studied system and there are few published reports on the subject [7–9]. The electrodeposition of silver–copper is readily carried out from aqueous ammonia solutions. However, adherent deposits have not been obtained, only powders [9]. Moreover, the conditions of dendritic or nodular-cluster growth have not been explained.

In relation to EDTA and HEDTA, they are two similar aminopolycarboxylate ligands that can form complexes with silver(I) ions and copper(II) ions [10]. However, they can affect the silver–copper electrodeposition process differently, since different charged species can be formed at a given pH, leading to silver–copper deposits with distinct morphologies or compositions. We have investigated the use of EDTA [11] or HEDTA [12] in the silver-plating bath, with some excellent results, such as improved deposit morphology and suppression of the dendritic growth. Thus,

the aim of this study was to analyze the influence of EDTA and HEDTA on silver–copper electrodeposition from ammonium hydroxide solution.

2 Experimental details

All chemicals were analytical grade. The solutions were prepared with double-distilled water throughout. The electrochemical experiment was performed in freshly prepared plating solutions containing ammonia (NH_3), $AgNO_3$ and/or $Cu(NO_3)_2$, whose compositions are shown in Table 1. In addition, the effects of EDTA and HEDTA were studied. The basic solution composition of 1.0×10^{-1} mol L^{-1} $Cu(NO_3)_2$ + 5.0×10^{-1} mol L^{-1} NH_3 + 1.0 mol L^{-1} $NaNO_3$ was named BE_{Cu}. Silver–copper electrodeposition was carried out in BE_{Cu} containing no more than 5.0×10^{-2} M $AgNO_3$, since at $[Ag^+]$:$[Cu^{2+}]$ ratios higher than 2.0, a blue precipitate ($Cu(OH)_2$) was observed in preliminary lab.

Voltammetric and chronoamperometric curves were recorded with a GAMRY PCI-4 750 mA Potentiostat/Galvanostat. All experiments were carried out at room temperature (25 °C) with a stationary electrode, except in Fig. 4. A platinum disk (0.20 cm^2), a Pt plate and an appropriate Luggin capillary (containing Hg/HgO, 1.0 M NaOH) were employed as working, auxiliary and reference electrodes, respectively. Immediately before the electrochemical measurements, the working electrode was washed with a mixture of concentrated sulphuric and nitric acids and rinsed with double-distilled water. All values of current density were calculated with respect to the initial platinum electrode area (0.20 cm^2). The platinum substrate was only employed as working electrode due to its noble character.

Scanning Electron Microscopy (SEM) photographs were taken with a Philips FEG XL 30 microscope. Energy-dispersive X-ray spectroscopy (EDS) measurements were made with an eLX Oxford, EDS Si/Li, ultrathin Be window [13]. EDX analysis was carried over as much of the area of the electrode as possible, perpendicular to the surface, without reaching the Teflon surrounding the disc platinum electrode.

X-ray diffraction (XRD) patterns of the deposit surface were produced with Cu Kα radiation (1.5406 Å), using an X-ray Rigaku Rotaflex RU200B goniometer, in 2θ scanning mode (fixed $\omega = 2^\circ$) [14].

SEM, EDS and XRD were carried out on silver–copper deposits obtained potentiostatically with a step potential from +0.300 V to E_d.

3 Results and discussion

3.1 Chemical solution

The concentrations of the predominant species of silver(I) and copper(II) complexes in ammonia solution, without and with EDTA or with HEDTA, were calculated by the shooting method, attributing a value to the free ammonia concentration ($[NH_3]_f$) and calculating the concentrations of the other species (Table 2). This was made until the shot $[NH_3]_f$ was equal to the calculated $[NH_3]_f$, in an iterative process. The stability constants used for the complexes were: silver(I)-NH_3 ($\beta_1 = 10^{3.32}$ and $\beta_2 = 10^{7.24}$), copper(II)-NH_3 ($\beta_1 = 10^{4.12}$; $\beta_2 = 10^{7.63}$; $\beta_3 = 10^{10.51}$ and $\beta_4 = 10^{12.60}$), silver(I)-additive ($\beta_{1EDTA} = 10^{7.32}$ and $\beta_{1HEDTA} = 10^{6.71}$) and copper(II)-additive ($\beta_{1EDTA} = 10^{18.70}$ and $\beta_{1HEDTA} = 10^{17.5}$) [10] and the acidity of the solution was determined experimentally. The percentage of each species (P) was calculated by Eq. 1.

$$P_{M(L)_i}(\%) = \frac{[M(L)_i]}{\sum_{i=0}^{n} [M(L_1)_i] + [M(L_2)]} \times 100 \quad (1)$$

where, L_1 and L_2 are NH_3 and $EDTA^{4-}$ or $HEDTA^{3-}$, respectively. In solution without EDTA or HEDTA,

Table 1 Silver–copper electrodeposition solution compositions

	Electrodeposition solution, BE_{Cu}			
	$[AgNO_3]$ (10^{-2} mol L^{-1})	$[EDTANa_2]$ (10^{-3} mol L^{-1})	$[HEDTANa_3]$ (10^{-3} mol L^{-1})	pH
SAgCu1	0.10	–	–	10.04
SAgCu2	0.50	–	–	10.00
SAgCu3	1.0	–	–	9.96
SAgCu4	5.0	–	–	9.59
SAgCu5a	–	1.0	–	10.11
SAgCu5b	–	5.0	–	10.80
SAgCu5c	–	10.0	–	10.87
SAgCu6a	–	–	1.0	10.32
SAgCu6b	–	–	5.0	10.66
SAgCu6c			10.0	11.07

Table 2 Distribution of silver(I) and copper(II) species in ammonia (L_1) solution, without and with EDTA or HEDTA (L_2)

Electrodeposition solution	Chemical species in solution (%)			
	$[Ag(L_1)_2]^+$	$[Cu(L_1)_3]^{2+}$	$[Cu(L_1)_4]^{2+}$	$[Cu(L_2)]$
EB_{Cu}	–	84	91.5	–
SAgCu1	99.9	8.5	91.3	–
SAgCu2	99.8	9.2	90.6	–
SAgCu3	99.8	10.2	89.6	–
SAgCu4	99.4	28.5	69.6	–
SAgCu5a	99.5	23.6	74.1	1.0
SAgCu5b	99.7	17.0	77.4	5.0
SAgCu5c	99.7	12.3	77.4	10.0
SAgCu6a	99.5	23.6	74.1	1.0
SAgCu6b	99.7	17.0	77.4	5.0
SAgCu6c	99.7	12.3	77.4	10.0

$[M(L_2)]$ is zero. The maximum number of ligand (n) for silver(I) and copper(II) were 2 and 4, respectively.

It can be seen in Table 2 that the predominant silver(I) and copper(II) species are the diaminesilver(I) ($[Ag(NH_3)_2]^+$) and tetraaminecopper(II) ($[Cu(NH_3)_4]^{2+}$) complexes, irrespective of the solution composition. In addition, the added EDTA or HEDTA complexed mainly with copper(II) ion, decreasing the total concentration of the copper-NH_3 complexes. The voltammetric curves were correlated with the solution composition (Sect. 3.2.1).

3.2 Electrochemical experiments

3.2.1 Voltammetric study

Figure 1 shows voltammetric curves for silver and copper electrodepositions onto a platinum substrate from ammonium hydroxide solution containing silver(I) or copper(II) ion. Silver voltammetric deposition (Fig. 1, solid curve) was carried out in 5.0×10^{-2} mol L^{-1} $AgNO_3$ + 5.0×10^{-1} mol L^{-1} NH_3 + 1.0 mol L^{-1} $NaNO_3$ solution. In this solution, $[Ag(NH_3)_2]^+$ is the predominant species. The cathodic sweep (Fig. 1, solid curve) indicated that the $[Ag(NH_3)_2]^+$ was reduced at potentials more negative than +0.055 V (c_{Ag1} region), followed by an extended potential region where the current density was controlled by mass transport (c_{Ag2} region). The reaction that occurred in these regions was: $\left[Ag(NH_3)_2\right]^+_{(aq)} + e^- \rightleftharpoons Ag + 2NH_{3(aq)}$, which is influenced by the free ammonia concentration. Beyond these two regions, the current density increased again at potentials more negative than −0.630 V (c_{Ag3} region), owing to the hydrogen evolution reaction (HER), which occurred in parallel with silver deposition. In the reverse sweep, the silver dissolution process (a_{Ag1} region) occurred at potentials more positive than +0.140 V, showing a single peak at +0.350 V.

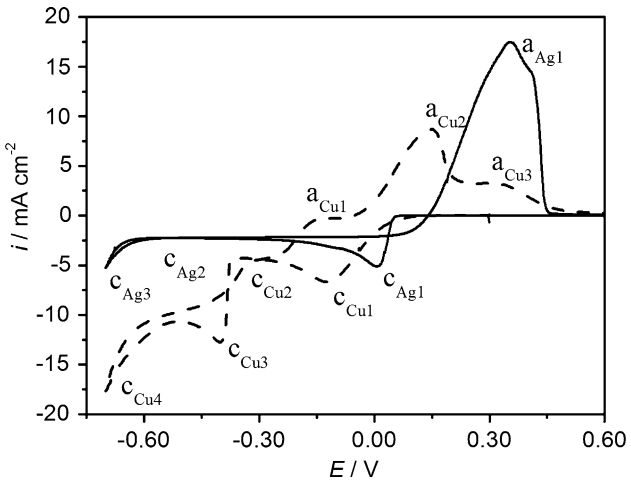

Fig. 1 Voltammetric curves for: (——) silver deposition and (– – –) copper deposition on a platinum substrate. $\upsilon = 10.0$ mV s^{-1}

Copper voltammetric deposition (Fig. 1, dashed curve) was carried out in BE_{Cu} solution. In this solution, $[Cu(NH_3)_4]^{2+}$ is the predominant species (Table 2). In the cathodic sweep, the current density increased slowly at potentials more negative than +0.100 V up to −0.200 V (c_{Cu1} region) representing the reduction of $[Cu(NH_3)_4]^{2+}$ to $[Cu(NH_3)_2]^+$ [15], after which the current density decreased, owing to the diffusion-limited mass transport (c_{Cu2} region). Applying the Tafel equation to the first region of copper reduction confirmed that this process was monoelectronic, since, assuming a transfer coefficient (α) of 0.50, a number of electrons transferred (n) equal to 1.0 was obtained. Moreover, in the voltammetric curve obtained in a stirred solution with the rotating disc electrode and reversing the cathodic sweep at −0.200 V (figure not shown in this paper), no peak was observed in the anodic polarization. This result indicated that the species formed at this region of potential was soluble in the

solution, i.e. $[Cu(NH_3)_2]^+$. Bulk copper deposition occurred at potentials more negative that −0.377 V (Fig. 1, dashed curve, c_{Cu3} region), initially by reduction of $[Cu(NH_3)_2]^+$ and then, after these ions were depleted at the surface of the electrode, by the direct reduction of $[Cu(NH_3)_4]^{2+}$ [15]. The HER occurred at potentials more negative than −0.500 V (c_{Cu4} region). In the anodic sweep, three regions were seen: a shoulder at −0.150 V (a_{Cu1} region), a peak at +0.150 V (a_{Cu2} region) and another shoulder at +0.330 V (a_{Cu3} region). The a_{Cu1} region was probably related to oxidation of metallic copper to $[Cu(NH_3)_2]^+$. In the a_{Cu2} region, the $[Cu(NH_3)_2]^+$ complex was oxidized to $[Cu(NH_3)_4]^{2+}$. The a_{Cu3} region may be related to direct oxidation of metallic copper to $[Cu(NH_3)_4]^{2+}$ [15]. These voltammetric curves indicated that the silver deposition process is controlled by mass transport at the potential where bulk copper deposition (−0.377 V) occurs, implying that silver and copper codeposition is possible. Moreover, a high overpotential is required to obtain silver–copper deposits. Hence, this could lead to silver–copper deposits composed of dendrites, an idea that was verified by SEM (Sect. 3.3).

Figure 2 shows voltammetric curves for silver–copper electrodeposition from BE_{Cu} solutions without and with various $AgNO_3$ concentrations. The predominant species in these solutions were $[Ag(NH_3)_2]^+$ and $[Cu(NH_3)_4]^{2+}$ (Table 2). The voltammetric curves obtained in BE_{Cu} (solid curve), SAgCu1 (dashed curve), SAgCu2 (dotted curve) and SAgCu3 (dashed-dotted curve) were not significantly different with respect to the deposition onset potentials or current density. This may be due to the reduction potentials of $[Ag(NH_3)_2]^+$ and $[Cu(NH_3)_4]^{2+}$ being very close and the current density for $[Ag(NH_3)_2]^+$ reduction being much smaller than that for $[Cu(NH_3)_4]^{2+}$ reduction. Moreover, as the $[Ag(NH_3)_2]^+$ concentrations were lower than in Fig. 1, it is important to consider the concentration polarization that shifted the deposition potential of silver negatively. On the other hand, in SAgCu4 (Fig. 2, dashed-dotted-dotted curve), the voltammetric curve was significantly different from the others, showing a higher current density. In this case, five cathodic regions can be distinguished (c_{AgCu1}, c_{AgCu2}, c_{AgCu3}, c_{AgCu4}, and c_{AgCu5}), which were related to the individual $[Ag(NH_3)_2]^+$ and $[Cu(NH_3)_4]^{2+}$ reductions. It was noted that the peak potentials for $[Ag(NH_3)_2]^+$ (c_{AgCu1} region) and $[Cu(NH_3)_4]^{2+}$ (c_{AgCu2} region) reductions were shifted positively by about 32 and 13 mV, respectively. This shift may be attributed to a decrease in free ammonia concentration compared to the individual depositions (Fig. 1). In the c_{AgCu1} region the current density increased steeply from +0.100 V, with a peak at +0.040 V, mainly due to $[Ag(NH_3)_2]^+$ reduction. After this, the current density increased again, showing another peak at −0.100 V (c_{AgCu2} region) and then decreased between

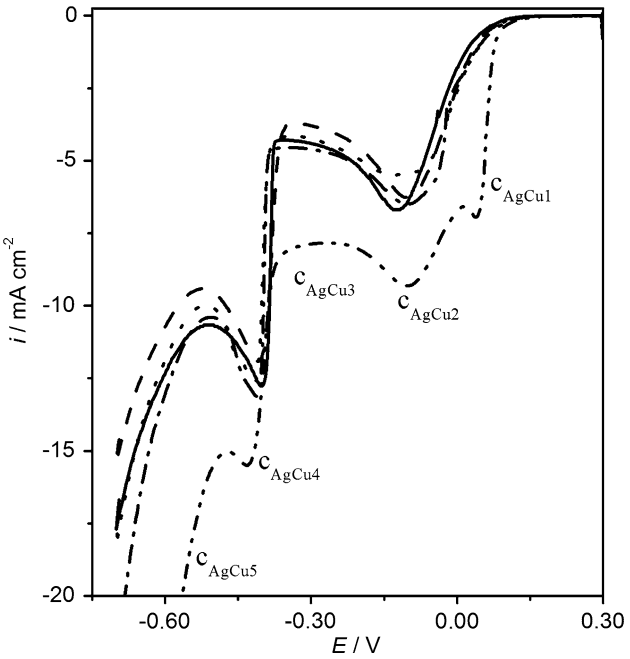

Fig. 2 Cathodic voltammetric curves for silver–copper deposition on a platinum substrate from: (——) BE_{Cu}; (– – –) SAgCu1; (· · ·) SAgCu2; (– · –) SAgCu3 and (– · · –) SAgCu4. $\upsilon = 10.0$ mV s^{-1}

−0.100 and −0.375 V (c_{AgCu3} region), indicating $[Cu(NH_3)_4]^{2+}$ reduction to $[Cu(NH_3)_2]^+$. The bulk silver–copper deposition and HER occurred at potentials more negative than −0.375 V (c_{AgCu4} region) and −0.500 V (c_{AgCu5} region), respectively.

In light of the fact that a high overpotential (about 0.48 V) can lead to dendritic growth, the influence of EDTA or HEDTA on the silver–copper electrodeposition process was studied in 5.0×10^{-2} M $AgNO_3 + BE_{Cu}$ solution, since these additives have shown excellent results in suppressing silver dendritic growth [11, 12].

Figure 3a and b show voltammetric curves in solutions containing various EDTA and HEDTA concentrations. In these solutions $[Ag(NH_3)_2]^+$ and $[Cu(NH_3)_4]^{2+}$ (Table 2) are the predominant species. It must be stressed that EDTA and HEDTA formed complexes mainly with copper(II) (Sect. 3.1). The voltammetric curve in SAgCu5a (Fig. 3a) shows that the peak current densities in the c_{AgCu1} and c_{AgCu4} regions were higher than in the solution without additive (SAgCu4), while in SAgCu5b and SAgCu5c, the current density was smaller in these regions. In addition the current density in the c_{AgCu2} and c_{AgCu3} regions did not change significantly, indicating that EDTA possibly did not affect the reduction of $[Cu(NH_3)_4]^{2+}$ to $[Cu(NH_3)_2]^+$. On the other hand, in the solutions containing HEDTA (Fig. 3b), the current density in the c_{AgCu1} and c_{AgCu4} regions increased in SAgCu6a and SAgCu6b, decreasing only in SAgCu6c. These changes in the current densities

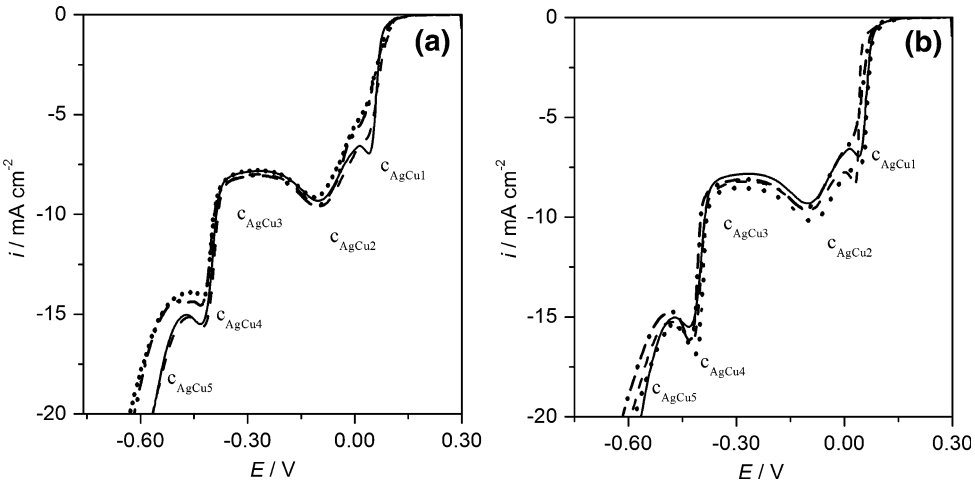

Fig. 3 Voltammetric curves for silver–copper deposition on a platinum substrate from solutions without and with various (**a**) EDTA and (**b**) HEDTA concentrations: (——) SAgCu4; (– – –) SAgCu5a or SAgCu6a; (· · ·) SAgCu5b or SAgCu6b and (– · –) SAgCu5c or SAgCu6c. $\upsilon = 10.0$ mV s^{-1}

(c_{AgCu1} and c_{AgCu4} regions) may have been caused by the changes in the distribution of copper(II) species (Table 2) and changes in the deposit morphology (see SEM, Sect. 3.3). Moreover, these results showed that EDTA and HEDTA affected the silver–copper electrodeposition differently with respect to their concentrations.

To obtain further information about the effects of EDTA and HEDTA, voltammetric curves with the rotating disc electrode were carried out in 5.0×10^{-2} M $AgNO_3$ + BE_{Cu} solutions without and with 1.0×10^{-2} M EDTA or 1.0×10^{-2} M HEDTA. Plots of i^{-1} versus $\omega^{-1/2}$ (ω = angular velocity) were drawn for −0.200 and −0.500 V (Fig. 4a and b). From these plots, the current density of charge transfer (i_{ct}) was estimated applying Eq. 2 [16]:

$$\frac{1}{i_t} = \frac{1}{i_{ct}} + \frac{1}{i_{mt}} = \frac{1}{i_{ct}} + \frac{1}{B\omega^{1/2}} \quad (2)$$

where i_t, i_{mt} and B are the total current density at −0.200 or −0.500 V, current density of mass transport and mass transport coefficient, respectively. Figure 4a and b show that all plots were linear, except that obtained at −0.500 V from SAgCu4. In this case, the plot was not linear for high ω, probably because of the silver–copper dendritic growth, which increased the current significantly. Table 3 shows i_{ct} and B values for silver–copper electrodeposition. It can be seen that i_{ct} was smaller in SAgCu5c and SAgCu6c than in solution without additive (SAgCu4), indicating that EDTA and HEDTA were probably adsorbed on the Pt substrate and silver–copper electrodeposit. On the other hand, B did not vary, indicating that the additive had no effect on the mass transport of the cations, suggesting that silver(I) and copper(II) reductions occurred from $[Ag(NH_3)_2]^+$ and $[Cu(NH_3)_4]^{2+}$.

3.2.2 *Chronoamperometric study*

In light of the voltammetric results, chronoamperometry studies were performed by stepping the potential from +0.300 to −0.450 V, since the bulk silver–copper deposition occurred only in the c_{AgCu4} region.

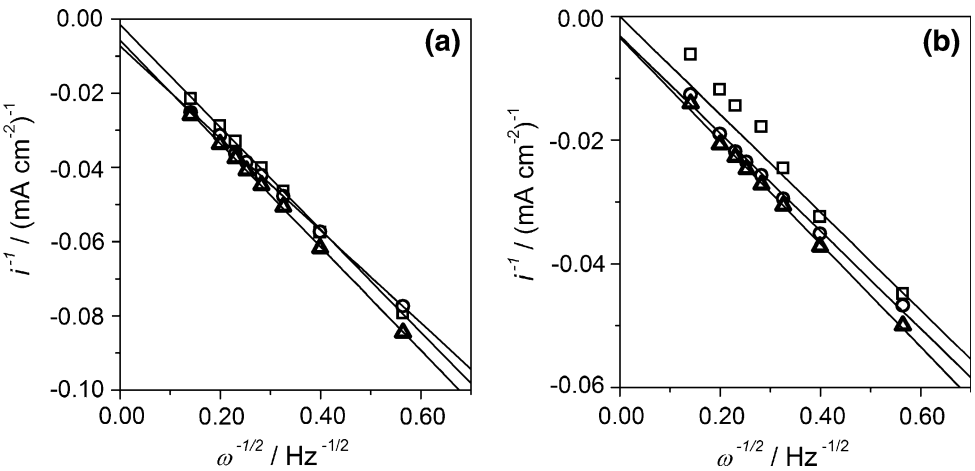

Fig. 4 Plots of i^{-1} versus $\omega^{-1/2}$ for voltammetric deposition of silver–copper on a rotating disc electrode from: (□) SAgCu4; (*o*) SAgCu5c and (Δ) SAgCu6c at potentials of (**a**) −0.200 V and (**b**) −0.500 V

Table 3 Values of current density of charge transfer (i_{ct}) and mass transfer coefficient (B) for silver–copper electrodeposition

Electrodeposition solution	−0.200 V		−0.500 V	
	i_{ct} (mA cm^{-2})	B (mA s$^{1/2}$ cm^{-2})	i_{ct} (mA cm^{-2})	B (mA s$^{1/2}$ cm^{-2})
SAgCu4	666	7.2	500	12
SAgCu5c	137	8.2	318	13
SAgCu6c	175	7.2	292	12

Figure 5 shows chronoamperometric curves for silver, copper and silver–copper depositions at −0.450 V from solutions without EDTA and HEDTA. In silver electrodeposition (Fig. 5, solid curve), the current density remained constant up to about 8.0 min, depositing 1.6 C cm^{-2}. This indicated that probably up to this deposition charge density, the silver deposit morphology probably did not suffer great changes with respect to its initial features. From this time, the current density increased because of dendritic growth of silver (confirmed by SEM, see Fig. 7b), which increased the actual surface area of the electrode. On the other hand, in the copper electrodeposition (Fig. 5, dashed curve), the current density was constant up to 30 min (deposition of 10.5 C cm^{-2}), indicating no significant change in the deposit morphology from its initial features. The chronoamperometric curves for silver–copper electrodeposition from SAgCu1 (Fig. 5, dotted curve), SAgCu2 (Fig. 5, dashed-dotted curve) and SAgCu3 (Fig. 5, dashed-dotted-dotted curve) showed similar features to the copper electrodeposition, but with bigger current density. Conversely, the silver–copper electrodeposition from SAgCu4 (Fig. 5, dashed-dashed-dotted curve) was similar to the silver electrodeposition, but with a higher current density. The current transient in SAgCu4 indicated that the dendritic growth probably occurred after about 6.5 min (4.8 C cm^{-2}) and suggested that this deposit has a high silver content (confirmed by EDS, Sect. 3.3). In addition to these results, it was found that, after a long time of deposition from SAgCu3, the current density increased by about 6% (seen in a magnification of Fig. 5, dashed-dotted-dotted curve not shown here), and thus was attributed to the change of morphology (seen in Fig. 8c, Sect. 3.3). On the other hand, the increase in current density was about 400% in SAgCu4. The silver–copper electrodeposit became dendritic at higher charge density because the process is controlled by mass transport. After a long deposition time diffusion zones are formed around the growth sites and dendritic growth is favored. This is related to the high charge-transfer current density in this silver–copper electrodeposition system (Table 3).

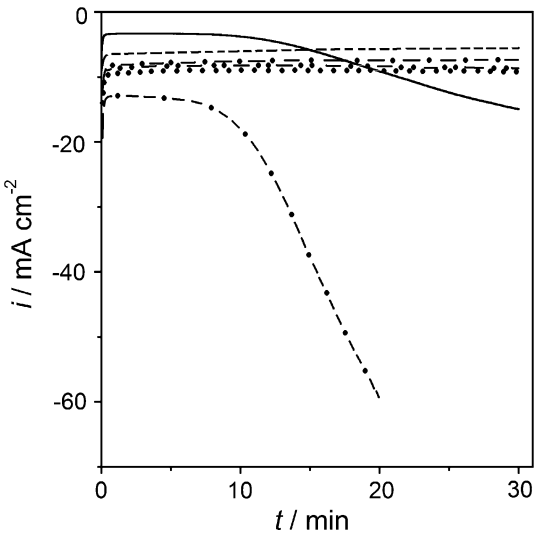

Fig. 5 Chronoamperometric curves for silver, copper and silver–copper deposition on a platinum substrate from: (——) 5.0 × 10^{-2} mol L^{-1} $AgNO_3$ + 5.0 × 10^{-1} mol L^{-1} NH_3 +1.0 mol L^{-1} $NaNO_3$; (– – –) BE_{Cu}; (· · ·) SAgCu1; (– · –) SAgCu2; (– · · –) SAgCu3 and (· – – ·) SAgCu4

Figure 6a and b show chronoamperometric curves for silver–copper electrodeposition at −0.450 V from 5.0 × 10^{-2} M $AgNO_3$ + BE_{Cu} solution, without and with various EDTA (Fig. 6a) and HEDTA (Fig. 6b) concentrations. Figure 6a indicates that in SAgCu5a (dashed curve) the dendritic growth begins after 5.0 min, prior to that in solution without additive (SAgCu4). On the other hand, in SAgCu5b (dotted curve) and SAgCu5c (dashed-dotted curve), the current densities were lower than those in SAgCu4 and SAgCu5a and the dendritic growth began probably at about 12 min (8.3 C cm^{-2}). Consequently, it was possible to obtain non-dendritic deposits with higher charge densities than that in the solution without additive (verified by SEM, Sect. 3.3). In the solution containing HEDTA (Fig. 6b), a slight inhibition of silver–copper dendritic growth occurred only in the solution containing 1.0 × 10^{-2} mol L^{-1} HEDTA (SAgCu6c).

These results show that EDTA and HEDTA have different effects on the silver–copper electrodeposition. Moreover, the inhibition of dendritic growth was probably due to EDTA and HEDTA adsorption on the Pt substrate

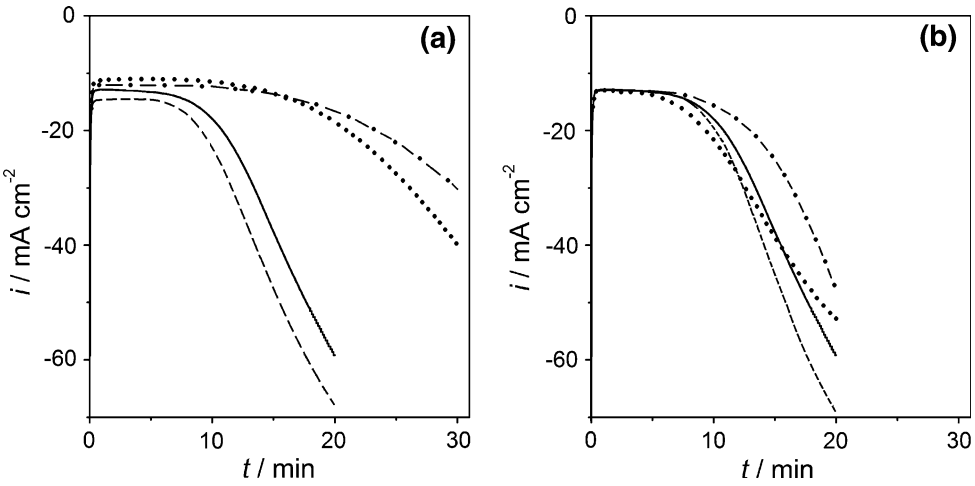

Fig. 6 Chronoamperometric curves for silver–copper deposition on a platinum substrate from solutions containing: **a** EDTA. **b** HEDTA: (——) SAgCu4; (– – –) SAgCu5a or SAgCu6a; (· · ·) SAgCu5b or SAgCu6b and (– · –) SAgCu5c or SAgCu6c

and silver–copper electrodeposit, decreasing the charge-transfer current density (Table 3).

3.3 SEM and EDS study

SEM and EDS were used to verify the hypotheses made in the chronoamperometric studies (Sect. 3.2.2). SEM and EDS were also used to assess the influence of the solution composition on the silver–copper morphology and composition.

SEM micrographs of the copper and silver deposits obtained at −0.450 V and with 10.0 C cm^{-2} are shown in Fig. 7a and b. The substrate is completely covered by smooth copper (Fig. 7a) and dendritic silver deposits (Fig. 7b). This corroborates the explanation given in Sect. 3.2.2 for the solid curve in Fig. 5, namely that the silver electrodeposition produces a dendritic deposit.

SEM micrographs of the silver–copper deposits obtained at −0.450 V with 10.0 C cm^{-2} are shown in Fig. 8a–d. The silver–copper deposits obtained from SAgCu1 (Fig. 8a), SAgCu2 (Fig. 8b) and SAgCu3 (Fig. 8c) formed at first a smooth three-dimensional layer, covering the substrate entirely with small globular crystallites. On this first layer, a second layer was formed, with an irregular scattering of globular crystallites (Fig. 8a and b) and clusters of nodular crystallites (Fig. 8c). The latter led to an increase in current density of about 6% (discussed in relation to Fig. 5). These results are in good agreement with the hypotheses based on the chronoamperometric studies (Sect. 3.2.2, Fig. 5), since this second layer probably did not change the actual area of the electrode significantly with respect to the first layer. The silver–copper electrodeposit obtained from SAgCu4 was composed of dendrites (Fig. 8d), similarly to the silver electrodeposit (Fig. 7b). EDS of the silver–copper deposits showed that the percentage of silver increased linearly with the silver concentration in the solution. The silver content in the deposit obtained from SAgCu4 was about 78 wt%, while for the other solutions it was lower than 20 wt%. This result points to the possibility of producing a silver–copper deposit of any desired composition by modifying the solution composition. In addition, it was confirmed that dendritic growth in a silver–copper deposit is related to high silver content.

The influence of EDTA or HEDTA on the silver–copper morphology and composition was studied in plating solutions containing 5.0×10^{-2} M $AgNO_3$. It was assumed that if the dendritic growth could be inhibited under the conditions that most favored it, the same effect could be expected under those conditions in which it was less favored, that is, in solution with lower $AgNO_3$ concentrations and at smaller overpotentials.

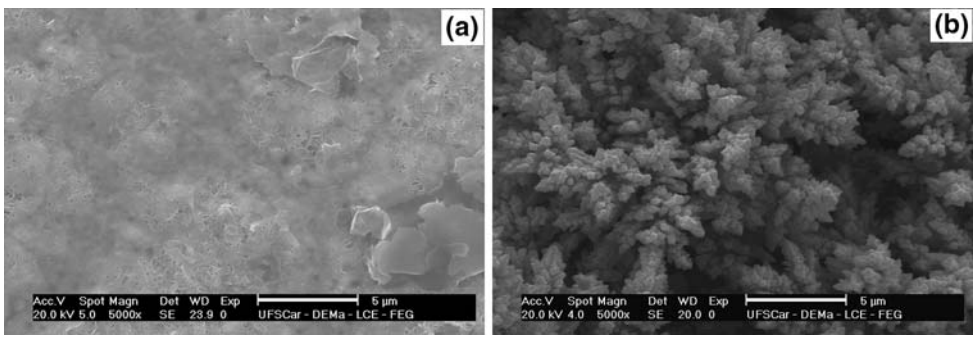

Fig. 7 SEM micrographs of copper and silver deposits on platinum substrate obtained at −0.450 V, with $q_d = 10.0$ C cm^{-2}, from: **a** BE_{Cu}. **b** 5.0×10^{-2} mol L^{-1} $AgNO_3 + 5.0 \times 10^{-1}$ mol L^{-1} $NH_3 + 1.0$ mol L^{-1} $NaNO_3$ solutions

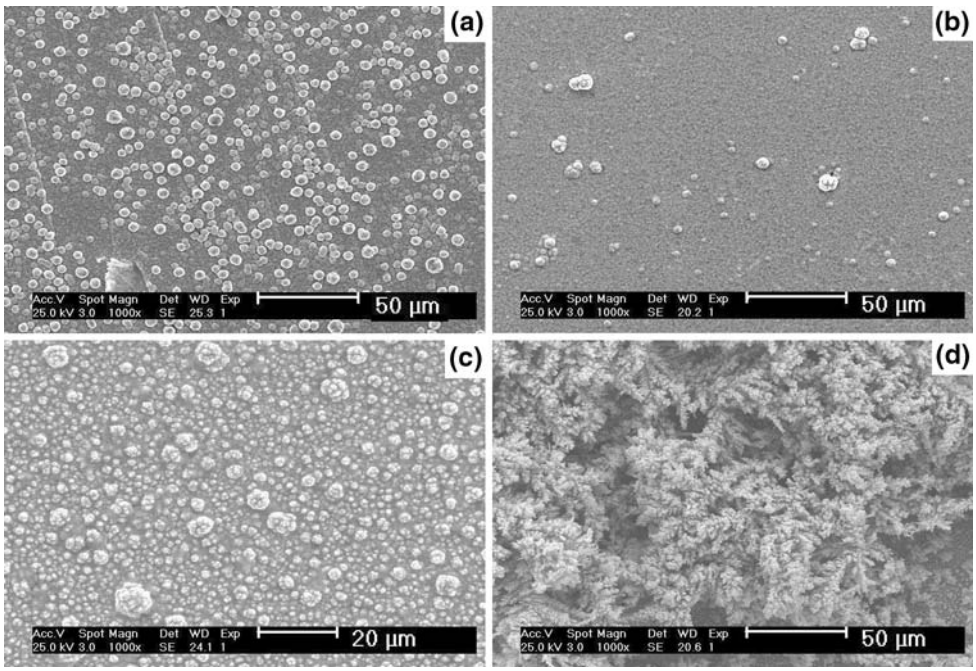

Fig. 8 SEM micrographs of silver–copper electrodeposits on platinum substrate obtained at −0.450 V, with $q_d = 10.0$ C cm^{-2}, from: **a** SAgCu1. **b** SAgCu2. **c** SAgCu3. **d** SAgCu4

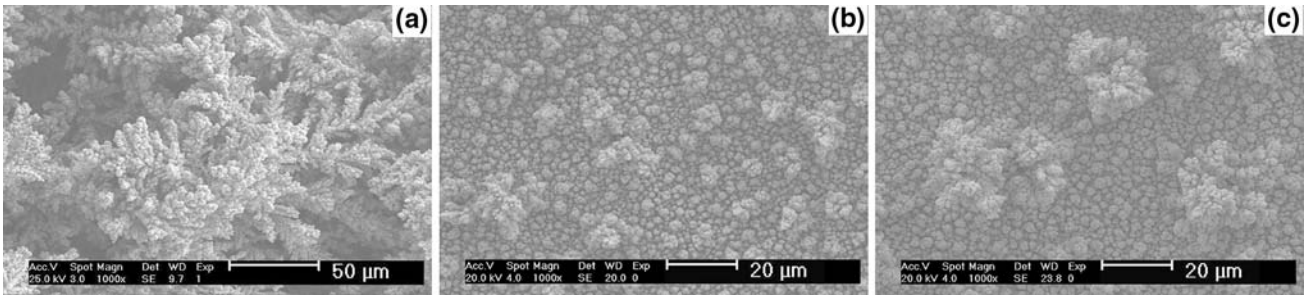

Fig. 9 SEM micrographs of silver–copper electrodeposits on platinum electrode obtained at −0.450 V, with $q_d = 10.0$ C cm^{-2}, from: **a** SAgCu5a. **b** SAgCu5b. **c** SAgCu5c

Figure 9a–c show the effect of EDTA on the silver–copper deposit morphology. EDTA affected the morphology, especially of deposits obtained from SAgCu5b (Fig. 9b) and SAgCu5c (Fig. 9c). This result is attributable to EDTA adsorption on the Pt substrate and silver–copper electrodeposit surface, decreasing charge-transfer current density (discussed in Fig. 4a and b, Sect. 3.2.1). HEDTA showed a similar effect on the silver–copper deposit morphology only in the solution containing 1.0×10^{-2} M HEDTA (SEM not shown in this paper). EDS indicated silver and copper codeposition and that EDTA and HEDTA affect the deposit composition, decreasing the silver content to about 55 wt% in the deposit obtained from SAgCu5c, compared to 78 wt% from SAgCu4. Considering the effects of EDTA and HEDTA on the silver(I) and copper(II) species distributions (Sect. 3.1), the opposite would be expected; that is, an increase in silver content. EDS analysis is affected by the homogeneity of the electrodeposit and differences in total composition can occur. This decrease in silver content was attributed to changes of silver, copper and silver–copper phase distribution in the deposit. Studies of dissolution voltammetry and atomic absorption spectroscopy of the solution obtained by chemical dissolution of the silver–copper electrodeposit indicated that EDTA and HEDTA affected the silver–copper phase distribution (results not shown here; to be published elsewhere). However, from the EDS results, it can be inferred that EDTA and HEDTA affect the composition of the silver–copper electrodeposit and the silver–copper electrodeposition process is regular.

The effect of charge density of deposition on the morphology and composition of the silver–copper electrodeposits was studied in SAgCu4 (Fig. 10a–c), SAgCu5c (Fig. 10d–f) and SAgCu6c (SEM not shown here). It can be seen in Fig. 10a–c that the morphology became dendritic on increasing the charge density. However, when EDTA

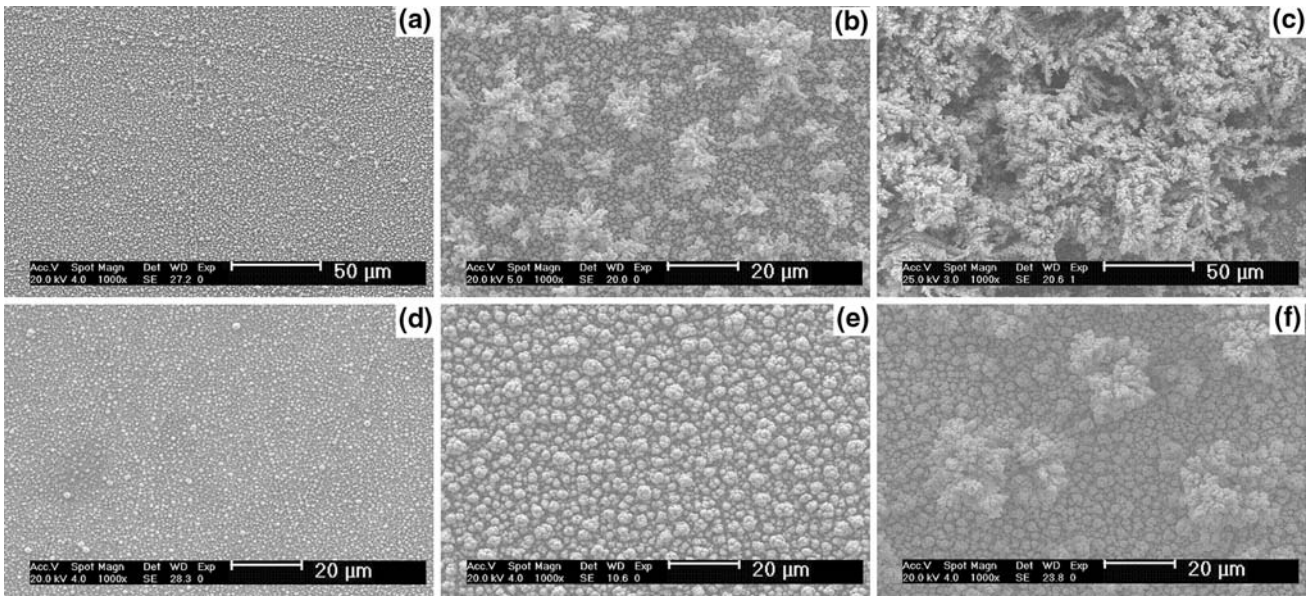

Fig. 10 SEM micrographs of silver–copper electrodeposits on platinum substrate obtained at −0.450 V, with (**a**, **d**) 2.0 C cm^{-2}, (**b**, **e**) 5.0 C cm^{-2}, and (**c**, **f**) 10.0 C cm^{-2}, from: **a–c** SAgCu4. **d–f** SAgCu5c

(Fig. 10d–f) was added to the solution, the dendritic morphology appeared only with 10.0 C cm^{-2}, but to a lesser extent than from the solution without EDTA. Moreover, it was found that the silver–copper deposits obtained with 2.0 C cm^{-2} from solutions without or with EDTA were non-dendritic, even though there was a high silver content (72–78 wt% Ag). At 5.0 C cm^{-2}, the dendritic growth was observed only in the solution without additive. These results indicate that not only does the silver–copper morphology depend on the silver content, but it also depends on the EDTA concentration and deposition charge density. SEM for silver–copper electrodeposits obtained from HEDTA solutions are not shown in this paper because this additive showed a similar effect to EDTA. Finally, the inhibition of dendritic growth was attributed to EDTA and HEDTA being adsorbed on the silver–copper electrodeposit.

It must be stressed that these results corroborate the hypothesis made on the basis of the chronoamperometric curves (Sect. 3.2.2), that dendritic growth appears as the charge density increases, and should be reduced in deposits produced from solutions containing EDTA or HEDTA. In addition, the silver–copper electrodeposition process was regular, that is, controlled by mass transport and with preferential silver deposition.

SEM and EDS were carried out on deposits obtained at −0.200 V (a potential before bulk copper deposition)) from SAgCu1 (Fig. 11a); SAgCu4 (Fig. 11b); SAgCu5c (Fig. 11c) and SAgCu6c (Fig. 11d). The silver–copper deposits were non-dendritic when deposited from SAgCu1, but dendritic and incompletely covering the platinum substrate when deposited from SAgCu4. However, their compositions were very similar (about 87 wt% Ag). When the silver–copper electrodeposit was obtained from solution containing EDTA (Fig. 11c) or HEDTA (Fig. 11d), it completely covered the substrate with a deposit without dendrites, even though the silver content (about 93 wt%) was close to that obtained from solution without additive (87 wt%). These results indicate that EDTA and HEDTA act as brighteners, which can be attributed to the decrease in the charge-transfer current density (discussed in relation to Fig. 4a and b and Table 3).

The silver–copper codeposition at −0.200 V has been attributed to $[Cu(NH_3)_2]^+$ disproportionation to $[Cu(NH_3)_4]^{2+}$ and metallic copper [15], which was incorporated in the silver deposit. This is possible, since the charge density of deposition was high (10.0 C cm^{-2}) and the time of deposition was very long (more than an hour). Thus, the amount of disproportionated $[Cu(NH_3)_2]^+$ was high and metallic copper was incorporated into the silver deposit. This mechanism is not easy to identify by voltammetry with the potential reversed at −0.200 V, since the total charge density in this case is very small and the rate of $[Cu(NH_3)_2]^+$ disproportionation probably slow, resulting in a small amount of incorporated copper. Moreover, a mixture of silver (or α phase) and silver–copper supersaturated solid solution was formed (to be discussed elsewhere), resulting in a complex anodic branch for dissolution in the same solution as the electrodeposition.

These results show that EDTA and HEDTA improved the silver–copper morphology, in spite of the increase in the silver content, indicating that EDTA and HEDTA act as brighteners.

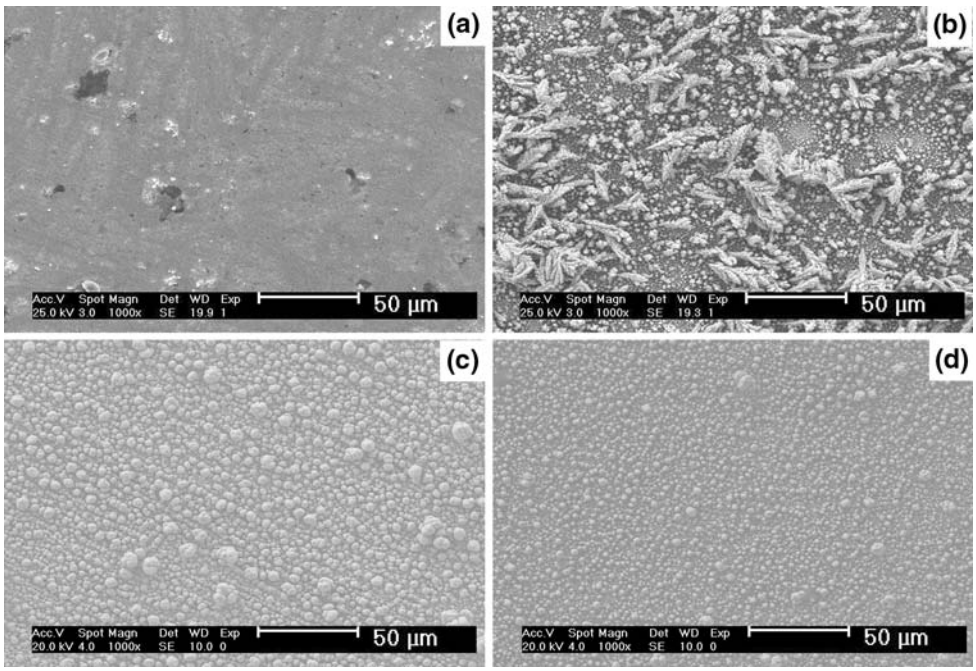

Fig. 11 SEM micrographs of silver–copper electrodeposits on platinum substrate obtained at −0.200 V, with $q_d = 10.0$ C cm^{-2}, from: **a** SAgCu1. **b** SAgCu4. **c** SAgCu5c. **d** SAgCu5d

3.4 X-ray diffraction analysis of the silver–copper deposits

X-ray diffraction was carried out on silver–copper deposits obtained at −0.450 V with 2.0 C cm^{-2}. The diffraction patterns of the electrodeposits were compared with the expected reflections for silver, copper and platinum [17], labeled in Fig. 12a and b as Ag, Cu and Pt, respectively.

Figure 12a show typical patterned diffraction for the silver–copper deposits obtained from SAgCu1, SAgCu2 and SAgCu3, which indicated that they were composed mainly of copper, exhibiting well-defined peaks for copper at the following reflections: (1 1 1), (2 0 0), (2 2 0), (3 1 1) and (2 2 2). In addition, on increasing the silver concentration in solution, and consequently in the silver–copper deposit, it was observed that the bases of the XRD peaks became broader (Fig. 12a and b), indicating that the deposits were less crystalline. This can probably be attributed to the deposition of silver–copper supersaturated solution [6]. On the other hand, the deposits obtained from SAgCu4, SAgCu5c and SAgCu6c (typical patterns in Fig. 12b) were composed mainly of silver, but did not exhibit well-defined peaks, indicating low crystallinity or formation of silver–copper supersaturated solid solution.

4 Conclusions

Silver–copper deposits were successfully obtained from ammonium hydroxide solution. Voltammetric studies indicated that silver deposition and copper(II) reduction to copper(I) occurred in the same potential region. Silver was deposited at potentials more negative than +0.100 V, while copper(II) was reduced to the copper(I) ion (beyond +0.100 V) and to metallic copper (beyond −0.380 V). Chronoamperometry, SEM and EDS indicated that increase of either silver content in the electrodeposit or charge density of deposition led to dendritic growth. Moreover, by raising the EDTA or HEDTA concentration, the dendritic growth was decreased. The silver–copper deposit produced at −0.200 V, from solutions containing EDTA or HEDTA, was non-dendritic. This inhibition of

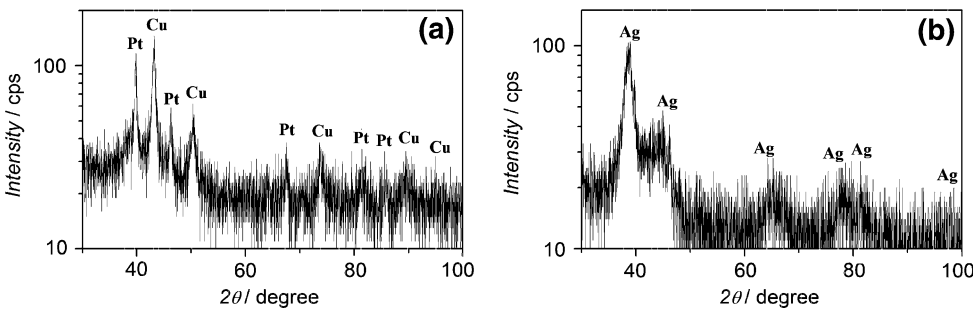

Fig. 12 Typical diffractograms of silver–copper electrodeposits on platinum substrate obtained at −0.450 V, from: **a** SAgCu1; SAgCu2 and SAgCu3. **b** SAgCu4; SAgCu5c and SAgCu6c. Standard X-ray diffraction lines of Ag (PDF-040783), Cu (PDF-040836) and Pt (PDF-040802) [17] are indicated

the dendritic growth was attributed to adsorption of the additive on the silver–copper electrodeposit surface. The copper and silver codeposition at −0.200 V was attributed to Cu(I) ion disproportionation to Cu(0) and Cu(II). EDTA and HEDTA additives work as brighteners. X-ray diffraction showed that the silver–copper electrodeposit was composed of supersaturated solid solution.

Acknowledgements Financial support from Brazilian agency FAPESP is gratefully acknowledged.

References

1. Cagran C, Wilthan B, Pottlacher G (2006) Thermochim Acta 445:104
2. Dettmer ZC, Persad C (2005) IEEE Trans Magn 41:176
3. Simon D, Bardolle J, Bujor M (1980) IEEE Trans Compon Hybrids Manuf Technol 3:13
4. Hansen M (1958) Constitution of binary alloys. McGraw-Hill Book Company, New York
5. Li ZQ, Shen H, Chen L, Li Y, Güther B, Korznikov AV, Valiev RZ (1996) J Phys D Appl Phys 29:1373
6. Sheng HW, Wilde G, Ma E (2002) Acta Mater 50:475
7. Rekcs W, Mrugalski T (1990) Plat Surf Finish 77:60
8. Brenner A (1963) Electrodeposition of alloys principles and practice. Academic Press, New York
9. Kuhn AT, Neufeld P, Yong K (1984) J Appl Electrochem 14:605
10. Kotrlý A, Šůcha L (1985) Handbook of chemical equilibria in analytical chemistry. Wiley, New York
11. de Oliveira GM, Barbosa LL, Broggi RL, Carlos IA (2005) J Electroanal Chem 578:151
12. de Oliveira GM, de Souza MR, Carlos IA (2007) J Mater Sci 42:10164
13. Goldstein JI, Roming AD Jr, Newbury DE, Lyman CE, Echlin P, Fiori C, Joy DC, Lifshin E (1992) Scanning electron microscopy and X-ray microanalysis: a text for biologists, materials scientists, and geologists. Plenum Press, New York
14. Cullity BD, Stock SR (2001) Elements of X-ray diffraction. Prentice-Hall, London
15. Grujicic D, Pesic B (2005) Electrochim Acta 50:4426
16. Bard AJ, Faulkner LR (1980) Electrochemical methods: fundamentals and applications. Wiley, New York
17. Joint Committee on Powder Diffraction Standards (JCPDS) (2000) In: International centre for diffraction data. Powder diffraction file PDF-2. Database Set 1-49. Pennsylvania, ICDD, CD-ROM